www.reading.ac.uk/centaur

CentAUR

Central Archive at the University of Reading

Reading's research outputs online

The Impact of Air-Sea Interactions on the Representation of Tropical Precipitation Extremes

L. C. Hirons[1,2] , N. P. Klingaman[1] , and S. J. Woolnough[1]

[1]Department of Meteorology, National Centre for Atmospheric Science, University of Reading, Reading, Berkshire, UK, [2]Department of Meteorology, University of Reading, Reading, Berkshire, UK

Abstract The impacts of air-sea interactions on the representation of tropical precipitation extremes are investigated using an atmosphere-ocean-mixed-layer coupled model. The coupled model is compared to two atmosphere-only simulations driven by the coupled-model sea-surface temperatures (SSTs): one with 31 day running means (31 d), the other with a repeating mean annual cycle. This allows separation of the effects of interannual SST variability from those of coupled feedbacks on shorter timescales. Crucially, all simulations have a consistent mean state with very small SST biases against present-day climatology. 31d overestimates the frequency, intensity, and persistence of extreme tropical precipitation relative to the coupled model, likely due to excessive SST-forced precipitation variability. This implies that atmosphere-only attribution and time-slice experiments may overestimate the strength and duration of precipitation extremes. In the coupled model, air-sea feedbacks damp extreme precipitation, through negative local thermodynamic feedbacks between convection, surface fluxes, and SST.

1. Introduction

Tropical precipitation extremes affect the livelihoods of billions of people: from severe flooding caused by the most extreme heavy rainfall events—such as that seen in southern India in November–December 2015—to severe drought caused by an unseasonal lack of rainfall—such as in southern Africa in December 2015. These extremes present a significant ongoing challenge to water resource planning.

General circulation models (GCMs), which are our best tools for understanding current and future changes in tropical precipitation extremes, generally agree that anthropogenic climate change is affecting the frequency and intensity of extremes (Senevirante et al., 2012). However, there remains considerable intermodel spread in the projected increase of precipitation extremes (Kharin et al., 2013), especially in the tropics (O'Gorman, 2015; O'Gorman & Schneider, 2009), where models often also underestimate the present-day frequency of extreme precipitation (e.g., Allan & Soden, 2008; Asadieh & Krakauer, 2015).

Much of the uncertainty in projections of tropical precipitation extremes ultimately stems from deficiencies in current, state-of-the-art GCMs. For example, deep convective systems, which produce the majority of tropical extreme rainfall, are not well represented (Rossow et al., 2013). Changes in tropical precipitation extremes have been shown to be more sensitive to changes to the model physics (e.g., to the convective parameterization) than a significant future warming perturbation (Wilcox & Donner, 2006).

Many studies investigating regional changes in tropical precipitation use atmosphere-only GCMs (AGCMs) with prescribed sea-surface temperatures (SSTs; e.g., Coppola & Giorgi, 2005; Deser & Phillips, 2009; Kopparla et al., 2013). However, such studies neglect two-way interactions between the atmosphere and the ocean. Not only can SST anomalies influence the stability of the atmospheric boundary layer and hence the strength and location of convection, but, through changing the surface fluxes of heat, moisture, and momentum, convective events can feedback on the ocean and change SST and ocean stratification. Air-sea interactions have been shown to affect the attribution of decadal precipitation change (e.g., Dong et al., 2017), as well as the representation of precipitation extremes in many tropical regions (e.g., reducing precipitation during peak rainfall in southern Africa; Ratnam et al., 2015).
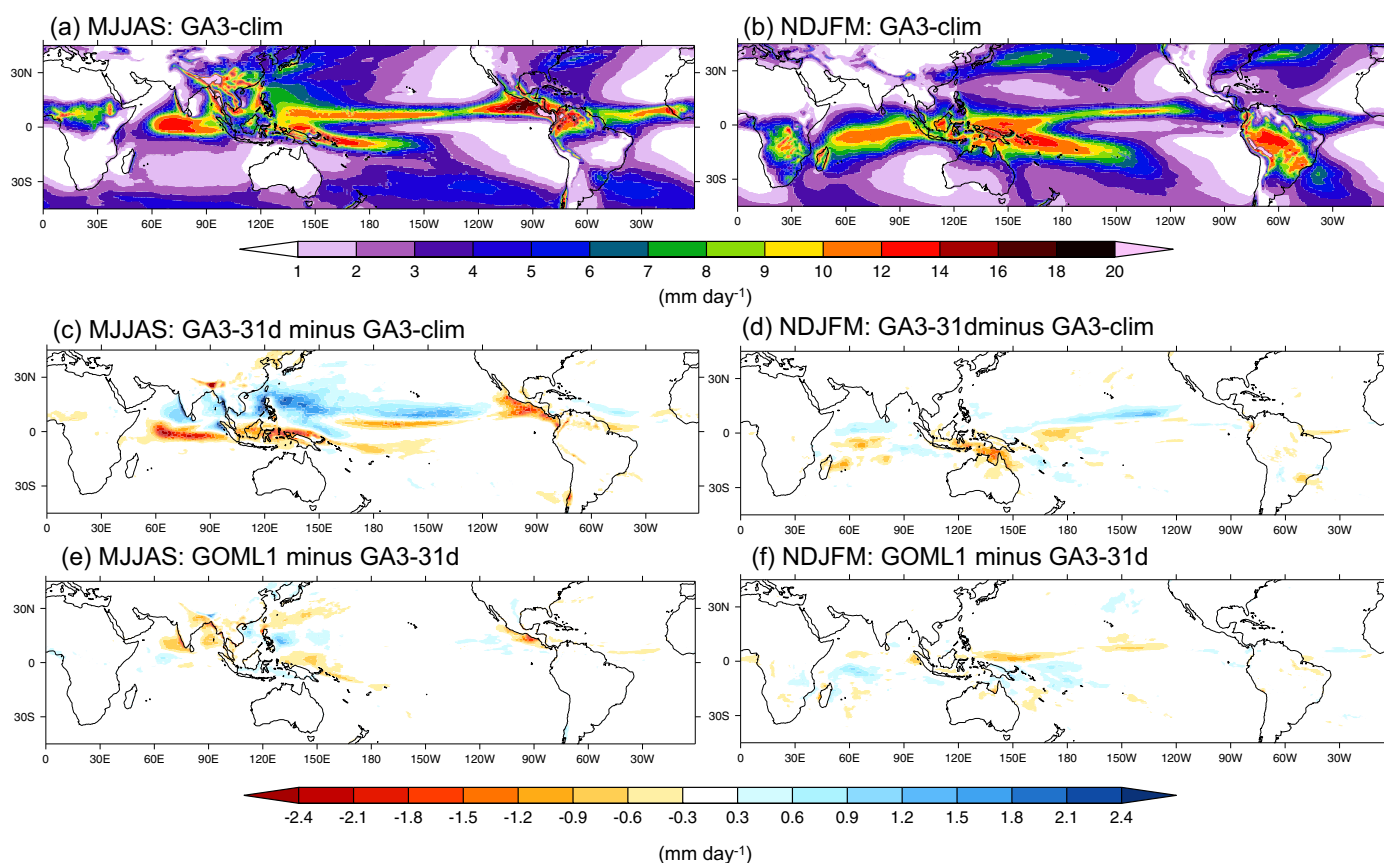
While such studies suggest that atmosphere-ocean GCMs with full dynamical oceans (AOGCMs) differ from AGCMs in their distributions of precipitation extremes, these differences are often complicated by large

changes in the mean state between AOGCMs and AGCMs, and should therefore be interpreted with caution. Additionally, air-sea interactions on subseasonal scales within such AOGCMs are often poorly resolved due to insufficient vertical ocean resolution and only a daily coupling frequency, which can degrade the representation of tropical subseasonal variability (e.g., Bernie et al., 2005; Klingaman et al., 2011; Tseng et al., 2015). The present study employs an AGCM coupled to many columns of a high vertical resolution ocean-mixed-layer model. Within this modeling framework air-sea interactions are well-resolved both spatially—the near-surface vertical resolution of the ocean is ∼1 m—and temporally—the atmosphere and ocean are coupled every 3 h. Furthermore, the application of ocean temperature and salinity corrections (section 2.1; Hirons et al., 2015) ensures the coupled model has a near-observed mean ocean state, which limits the impact of SST biases on the results. Therefore, this framework allows a clean identification of the impact of air-sea interactions on the representation of tropical precipitation extremes.

2. Model, Methods, and Data

2.1. Model

We use the Global Ocean-Mixed-Layer coupled configuration of the Met Office Unified Model (MetUM-GOML1; Hirons et al., 2015), comprising the MetUM Global Atmosphere 3.0 (GA3; Arribas et al., 2011; Walters et al., 2011) coupled to the Multi-Column K Profile Parameterization ocean (MC-KPP; see Hirons et al. (2015) for details), with a 3 h coupling frequency. Depth-varying temperature and salinity corrections, required to represent the mean oceanic advection and account for biases in the atmospheric surface fluxes, are applied to constrain the mean ocean state in MetUM-GOML toward the 1980–2009 climatology from the Met Office ocean analysis (Smith & Murphy, 2007). This results in minimal SST biases against observations (see Hirons et al., 2015, Figure 1b). The latitudinal extent of the air-sea coupling is defined by the maximum extent of

Figure 1. (a) GA3-clim MJJAS mean precipitation. Impact of interannual SST variability (c; GA3–31d minus GA3-clim) and air-sea coupling (e; GOML1 minus GA3–31d) on MJJAS mean precipitation. (b, d, f) As (a, c, e), but for NDJFM mean precipitation.

the seasonally varying sea-ice edge; beyond that the atmosphere is forced by the repeating mean annual cycle of SSTs from the Met Office ocean analysis above.

The simulations use N216 horizontal resolution, which is 0.83° longitude $\times$ 0.55° latitude with 85 points in the vertical and a model lid at 85 km. Three sets of simulations, each totaling 100 years (1 $\times$ 40 year and 2 $\times$ 30 year simulations), have been run. "GOML1" describes the MetUM-GOML1 coupled integrations. These are compared with two 100 year sets of GA3 simulations forced by (a) 31 day smoothed daily SSTs from GOML1 ("GA3–31d") and (b) a repeating mean annual cycle of daily climatological SSTs from GOML1 ("GA3-clim").

The framework used in this study enables a clean identification of the role that air-sea interactions play in the representation of tropical precipitation extremes. Within this framework, the impact of introducing interannual variability in SST in an atmosphere-only model (GA3–31d minus GA3-clim; hereafter referred to as "interannual SST variability") can be separated from the impact of introducing subseasonal air-sea feedbacks (GOML1 minus GA3–31d; hereafter referred to as "air-sea coupling"), using a model with a close-to-observed mean SST (Hirons et al., 2015).

2.2. Defining Extremes
Although there are many methods to define an extreme event (e.g., Schar et al., 2016), in its broadest sense a climate extreme is the occurrence of a climate variable above (or below) a threshold near the upper (or lower) tail of the observed distribution (Senevirante et al., 2012). The properties of such an extreme event can be characterized in terms of: (a) frequency—the number of times such a threshold is exceeded; (b) intensity—the magnitude by which the threshold is exceeded; and (c) persistence—the length of time the threshold is exceeded. We consider an example of each property of extreme precipitation. Of course, there is also subjectivity in the choice of an extreme threshold. This study aims to address this issue by applying a set of extreme diagnostics with different thresholds.

3. Results

Tropical precipitation extremes are considered in terms of (a) frequency using percentile thresholds (section 3.2), (b) intensity using return value thresholds (section 3.3), and (c) persistence using standard deviation thresholds (section 3.4). In this analysis, GA3-clim is used as a baseline climate and changes due to introducing interannual SST variability and air-sea coupling are assessed against that baseline. Before assessing the impact on tropical precipitation extremes, it is important to understand the impact of coupling and interannual SST variability on the mean rainfall, to interpret if differences in simulated extremes are due to shifts in the overall precipitation distribution caused by a change in the mean.
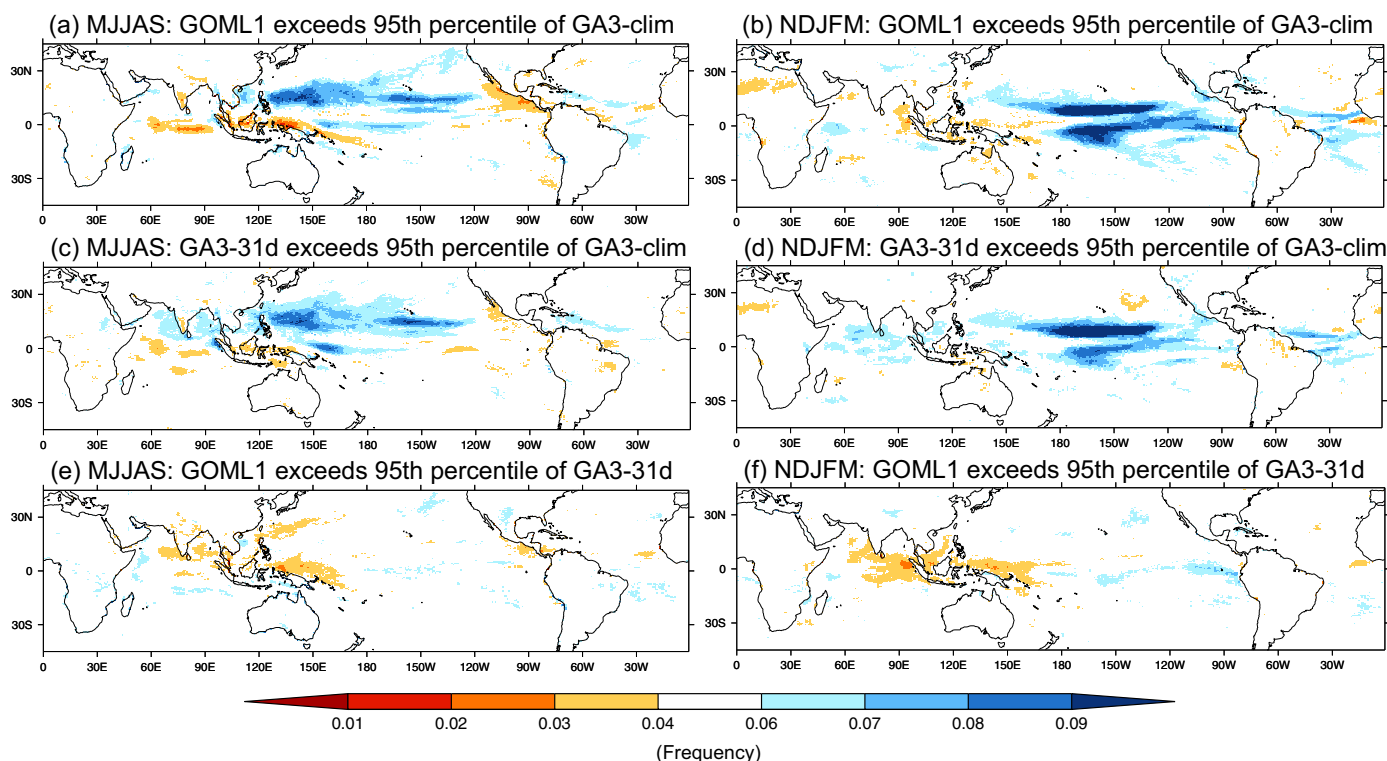
3.1. Impact of Air-Sea Interactions on Mean Rainfall
The seasonal migration of the Inter-tropical Convergence Zone (ITCZ) requires distinguishing between seasons when investigating the sensitivity of tropical precipitation extremes. Two seasons are considered: an extended summer (May–September, MJJAS) when the ITCZ lies north of the equator (Figure 1a); and an extended winter (November–March, NDJFM) when the ITCZ lies south of the equator (Figure 1b).

During MJJAS introducing interannual SST variability in MetUM-GA3 reduces precipitation in the equatorial Indian Ocean (IO) and Maritime Continent (MC) islands by more than 2 mm d^{-1} and increases precipitation further north, especially over the West Pacific (Figure 1c). This pattern suggests that the net effect of interannual SST variability is to shift the ITCZ slightly further north, which reduces biases in GA3-clim over the equatorial IO. However, it does not improve the underestimation of Indian summer monsoon rainfall, which is a long-standing MetUM bias (Johnson et al., 2015; Ringer et al., 2006). The spatial pattern of the impact of interannual SST variability during NDJFM is similar to MJJAS but much smaller in magnitude (Figure 1d). Air-sea coupling has little additional impact on mean precipitation in either season (Figures 1e and 1f). This analysis shows that, with the possible exception of the impact of interannual SST variability in MJJAS, the three simulations exhibit highly similar mean tropical precipitation.

3.2. Frequency
Changes in the frequency of tropical precipitation extremes are assessed using a threshold of the 95th percentile of daily precipitation. Figures 2a and 2b show the frequency with which the 95th percentile of

Figure 2. (a) GOML1 frequency of exceeding the daily MJJAS 95th percentile of GA3-clim precipitation. (c) As (a), but for GA3–31d exceeding the GA3-clim 95th percentile. (e) As (a), but for GOML1 exceeding the GA3–31d 95th percentile. (b, d, f) As (a, c, e), but for NDJFM.
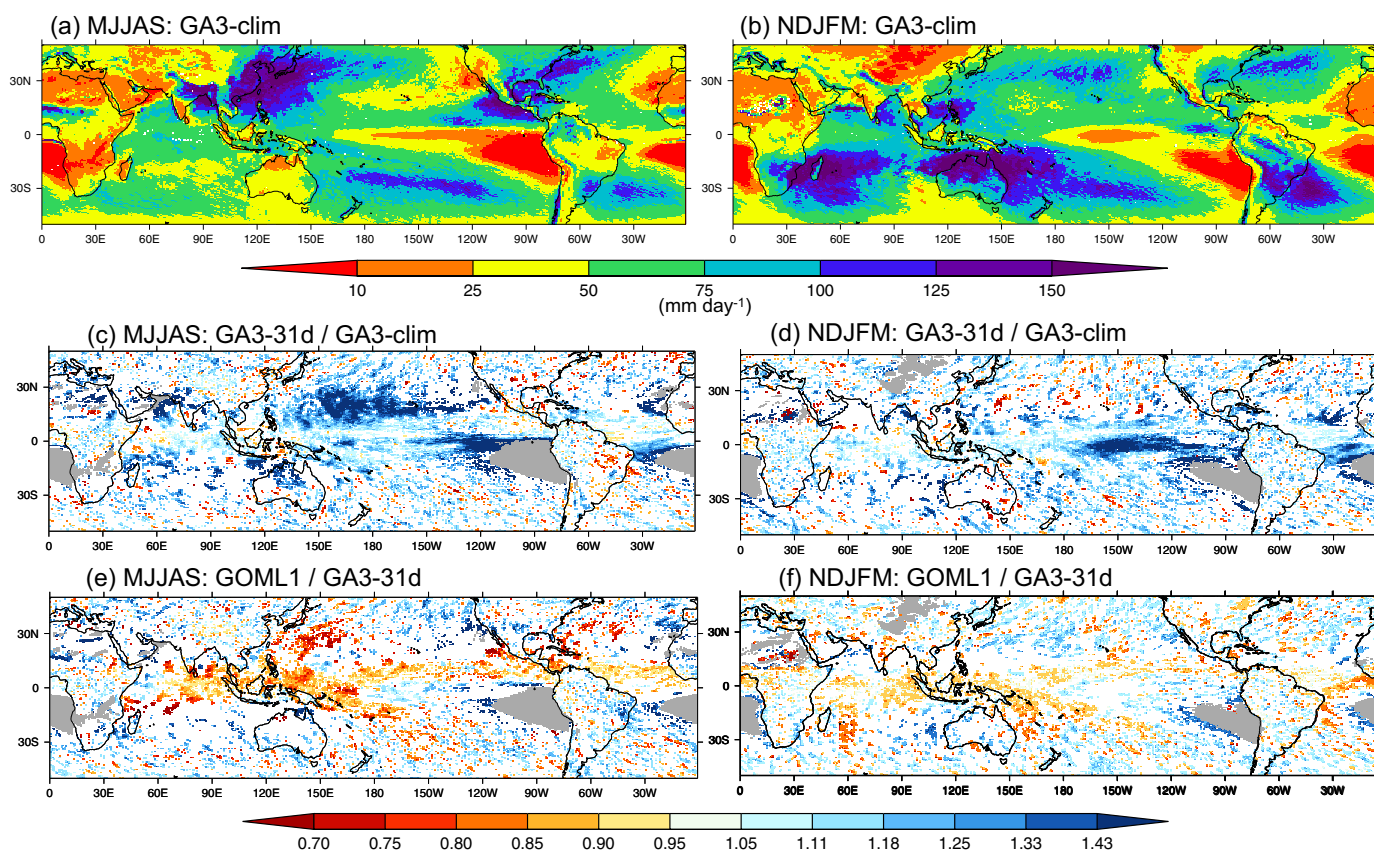
GA3-clim is exceeded by GOML1 during MJJAS and NDJFM, respectively. This total change is broken down into the impacts from interannual SST variability (Figures 2c and 2d) and air-sea coupling (Figures 2e and 2f). During MJJAS the total change in the 95th percentile (Figure 2a) shows an increase in extreme wet events in the western north Pacific, which is a result of interannual SST variability (Figure 2c), and a reduction in extreme wet events in the equatorial IO and MC region, which is largely a result of air-sea coupling. The spatial pattern of changes in the frequency of extremes in MJJAS is linked to changes in the mean MJJAS precipitation (Figure 1e).

This is not the case, however, in NDJFM: there was little change in mean precipitation but there are large changes in extremes across the tropical oceans. During NDJFM the interannual SST variability increases the frequency of wet events across the central Pacific (Figure 2d) while air-sea coupling reduces wet extremes across the IO and MC (Figure 2f). The change in Figure 2d is likely due to introducing interannual SST variability into the central Pacific. While MetUM-GOML lacks ocean dynamics and therefore cannot simulate the El Niño Southern Oscillation (ENSO), the model produces very weak thermodynamically driven ENSO-like SST variability around the dateline that can drive Indo-Pacific interannual precipitation variability.

Over land, where changes in tropical precipitation extremes will have the largest human impact, the small reduction in precipitation extremes over southern India in MJJAS (Figure 2a) and over northern Africa in NDJFM (Figure 2b) are a result of interannual SST variability (Figures 2c and 2d) rather than air-sea coupling.

3.3. Intensity

One method for analyzing climate extremes is to calculate the return value of a climate measure (x) by fitting a Generalized Extreme Value (GEV) distribution to the data at each grid point (e.g., Kharin et al., 2013, 2007). The maximum-likelihood method was used here for estimating the three GEV distribution parameters of location, scale, and shape. These parameters are then used to calculate the t-year return value which is the value that is exceeded by the climate measure x with probability $p = 1/t$. GEV analysis is applied to the seasonal maximum daily precipitation in MJJAS and NDJFM (i.e., to 100 values at each grid point for each

Figure 3. 20 year return values of MJJAS maximum of daily precipitation (P_{20}) from 100 years of GA3-clim simulation (a), mm d^{-1}. Ratio showing the impact of interannual SST variability on P_{20} (c; GA3–31d/GA3-clim) and the impact of air-sea coupling on P_{20} (e; GOML1/GA3–31d). The extreme value statistics are obtained by the maximum-likelihood method. (b, d, f) As (a, c, e), but for NDJFM P_{20}. Colored shading in Figures 3c–3f shows regions where the 95% confidence interval on the return values are completely separated. Grey shading masks regions where P_{20} is less than 10 mm d^{-1}.

100 year experiment). These have been applied to a range of t values but are shown for $t = 20$, to calculate a 20 year return value (P_{20}), or an annual exceedance probability of 5%.

The GEV analysis was applied to global precipitation in MJJAS and NDJFM, but coherent regions of significant changes were found only in the tropics. Figures 3a and 3b show P_{20} for GA3-clim MJJAS and NDJFM maximum precipitation. The largest values of P_{20}, above 150 mm d^{-1}, are located in the off-equatorial regions of the tropics and extratropics and mostly occur over the oceans. P_{20} values below 25 mm d^{-1} occur in regions of tropical marine stratocumulus off the west coast of Africa and South America and across northern Africa where there is very little total precipitation. There are further local minima, below 50 mm d^{-1}, over the MC islands and equatorial Pacific. The latitudinal migration of regions with the heaviest P_{20} follows the seasonal migration of the ITCZ (Figures 1a and 1b).

Figures 3c, 3d and 3e, 3f show the impact on P_{20} of interannual SST variability and air-sea coupling, respectively. Ratios are only shown where there is no overlap between the 95% confidence intervals of the two simulations. Figures 3c and 3d show that introducing interannual SST variability increases P_{20} across the tropical oceans; this is the expected thermodynamic effect given the nonlinear relationship between SST and precipitation (i.e., a warm SST anomaly will cause a larger-amplitude change in precipitation than a cold SST anomaly of the same magnitude; Spencer & Slingo, 2003). In MJJAS, there are also significant increases in P_{20} over northern Australia, the southeast Asian peninsula and parts of northern and eastern Africa. The largest increases in P_{20} are seen north of the equator in the western Pacific Ocean during MJJAS (Figure 3c). However, changes in extremes in this region during this season are likely partly due to an increase in mean precipitation there (Figure 1c). Air-sea coupling has the opposite effect of reducing P_{20} across the tropical Indo-Pacific (Figures 3e and 3f). This reduction is seen in both seasons and is most

coherent in the eastern IO and MC. There are also reductions in P_{20} over the southern tip of India in MJJAS and over North Africa in NDJFM. The reductions in the intensity of oceanic extremes with air-sea coupling are consistent with negative thermodynamic feedbacks occurring through the SST in the coupled system (i.e., an increase in convection increases surface fluxes out of ocean, which leads to a reduction in SST, a reduction in convection, and a reduction in the surface fluxes out of the ocean—a negative feedback). We explore these feedbacks further in section 3.4.

Although Figures 2 and 3 identify similar regions where tropical precipitation extremes are sensitive to air-sea coupling and interannual SST variability, the pattern correlations between these Figures are very small. The largest pattern correlation is 0.286 between Figures 2c and 3c.
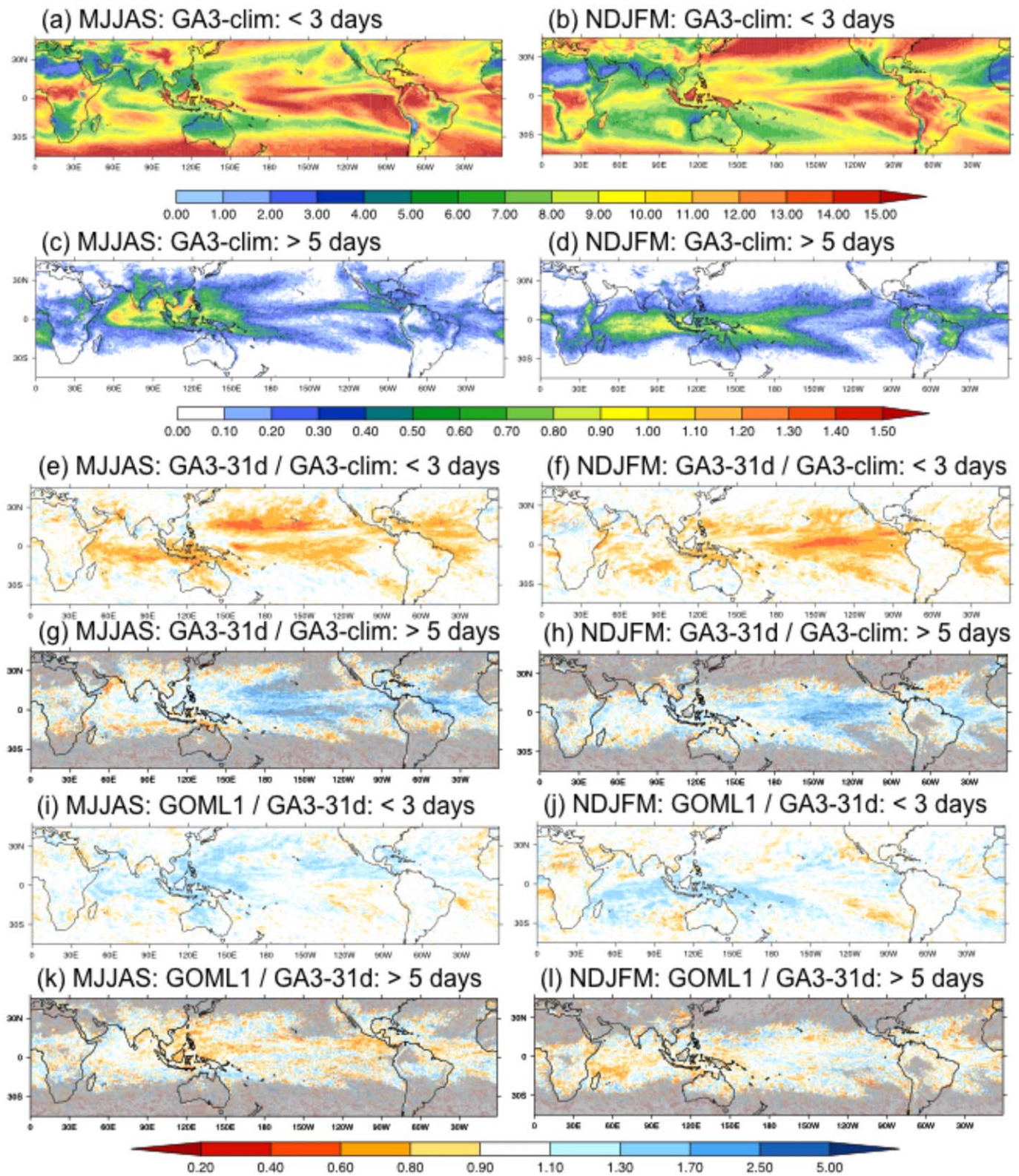
3.4. Persistence

While the intensity and frequency of extremes are important, it is often persistent extremes, where natural and human systems are under continued pressure, which have substantial social impacts. Changes in the persistence of precipitation extremes are measured by the frequency of consecutive days exceeding a particular threshold (Figure 4). The threshold, chosen to reflect local interannual variability, is one standard deviation from the daily climatological value. Although this is not the most intense threshold, it enables a sufficient sample size to draw meaningful conclusions from the data.

The analysis was initially carried out for the frequency of n consecutive days exceeding this precipitation threshold with $n = 1, \ldots, 10$. The clearest distinction was found among the simulations for $n < 3$ (less than 3 consecutive days; Figures 4a, 4b, 4e, 4f, 4i, and 4j and $n > 5$ (greater than 5 consecutive days; Figures 4c, 4d, 4g, 4h, 4k, and 4l); these are referred to as "short-lived" and "long-lived" extremes respectively and are the focus of the results shown here. During MJJAS and NDJFM, interannual SST variability reduces the frequency of short-lived extremes (Figures 4e and 4f) and increases the frequency of long-lived extremes (Figures 4g and 4h) over the tropical oceans. However, for both short-lived and long-lived extremes there is an increase in the total amount of precipitation falling in extreme events (not shown). This means that, although there are fewer short-lived extremes in GA3–31d compared with GA3-clim, those short-lived extremes are more intense. Interannual SST variability also reduces short-lived extremes over some tropical land regions, for example, central Australia, and southern Pakistan during MJJAS (Figure 4e) and over northwest Africa during NDJFM (Figure 4f). Increases in long-lived persistent extremes are evident over land regions of Borneo and northern South America during MJJAS (Figure 4g) and over Somalia and eastern Brazil during NDJFM (Figure 4h).
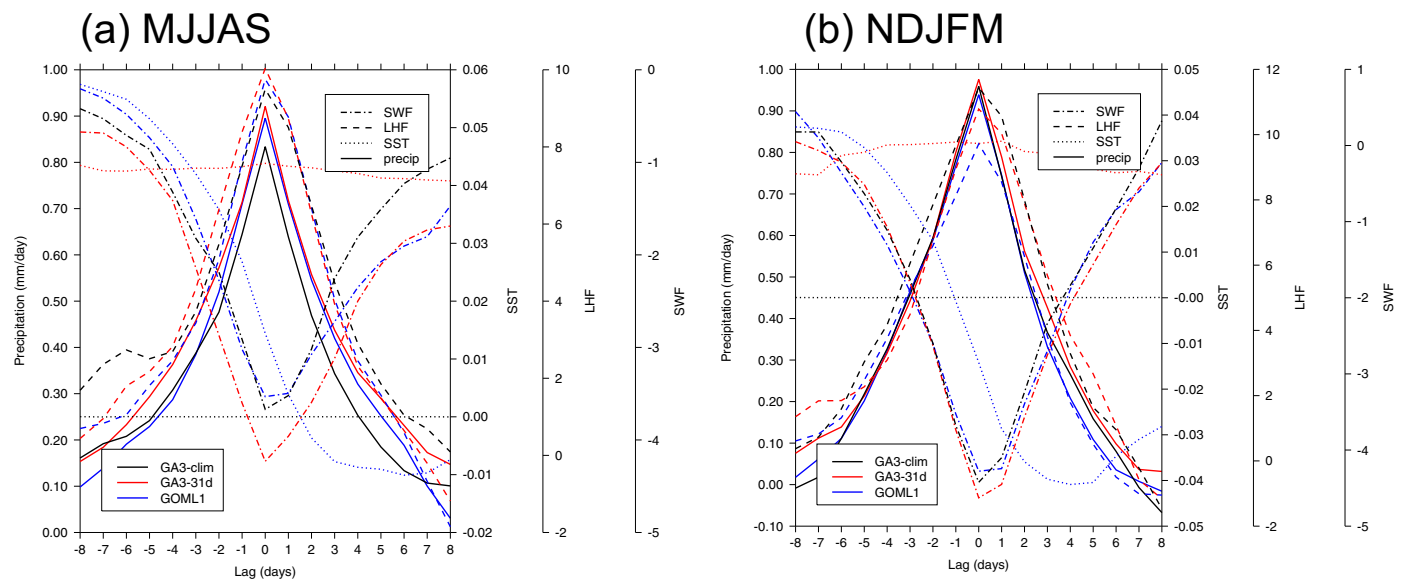
The impact of air-sea coupling is generally opposite to that of interannual SST variability, increasing the frequency of short-lived extremes (Figures 4i and 4j) and reducing the frequency of long-lived extremes (Figures 4k and 4l) over the tropical oceans. Air-sea coupling reduces the total precipitation falling in extreme events for both short-lived and long-lived extremes. Therefore, although there are more short-lived extreme events in GOML1 compared with GA3–31d, those short-lived extremes are less intense. The largest changes in the frequency of short-lived and long-lived extremes due to air-sea coupling are confined to the Indo-Pacific region and are colocated with regions of large mean rainfall in each season (Figures 1a and 1b). Over land, air-sea coupling increases short-lived precipitation extremes in central Australia and coastal Pakistan during MJJAS (Figure 4i) whereas it reduces short-lived extremes over northern Africa (Figure 4j) during NDJFM, although in this season this is a region of very low mean rainfall (Figure 1b).

The increase in persistence of oceanic extremes between GA3–31d and GA3-clim agrees with previous studies that have shown that increasing SST variability in atmosphere-only models induces strong positive subseasonal SST-surface-flux-precipitation relationships, which are inconsistent with the negative relationships found in observations (e.g., DeMott et al., 2015; Pegion & Kirtman, 2008; Rajendran & Kitoh, 2006). Introducing air-sea feedbacks damps these relationships through the negative thermodynamic feedbacks described in the previous section, reducing the persistence of precipitation extremes.

We assess the relationship between precipitation, SSTs, and surface fluxes during long-lived, persistent extremes in the tropical Indo-Pacific (Figure 5). The diagram shows composite anomalies for extreme events that persist above one standard deviation from the mean for at least 5 consecutive days (similar extreme definition as Figure 4). The peak in SST in GOML1 occurs up to 8 days before the maximum in precipitation, while in GA3–31d the SST anomalies are warm throughout the event. The associated maximum and

Figure 4. Frequency per year of (a, b) short-lived and (c, d) long-lived extremes for GA3-clim MJJAS and NDJFM mean. Short-lived and long-lived extremes are defined as less than 3 and greater than 5 days exceeding one standard deviation from the daily climatology, respectively. (e–h) show the impact of interannual SST variability (GA3–31d/GA3-clim) on (e, f) short-lived and (g, h) long-lived extremes during (e, g) MJJAS and (f, h) NDJFM. (i–l) The impact of air-sea coupling (GOML1/GA3–31d) on (i, j) short-lived and (k, l) long-lived extremes during (i, k) MJJAS and (j, l) NDJFM. Grey shading in (g, h, k, l) masks regions where the frequency of long-lived extremes is less than 0.1 yr^{-1}.

Figure 5. Lead-lag diagram of precipitation, SST, latent heat (LHF), and shortwave (SWF) flux anomalies during long-lived extreme events averaged over the Tropical Indo-Pacific [25S–25N, 60E–120W]. The definition of extreme here is similar to that of Figure 4—at least 5 consecutive days above one standard deviation from the mean. Lag 0 refers to the largest magnitude of that extreme event. GA3-clim, GA3–31d, and GOML1 are shown by the black, red, and blue lines, respectively.

minimum in latent heat flux (LHF) and shortwave flux (SWF), respectively, coincide with the maximum in precipitation. However, GA3–31d exhibits stronger negative SWF and positive LHF anomalies which persist for longer. In GOML1, the changes in surface fluxes lead to a clear cooling of SST during the extreme event. This negative thermodynamic feedback limits the event lifetime in GOML1 relative to GA3–31d. These findings are consistent with Figure 4.

4. Discussion and Conclusions

Changes in tropical precipitation extremes with air-sea coupling have been investigated in simulations with a coupled atmosphere-mixed-layer-ocean model and an atmosphere-only model driven by the coupled-model SSTs. Our experiment design allows the sensitivity to interannual SST variability to be separated from the presence of air-sea coupling feedbacks. The coupled model includes well-resolved air-sea interactions on subseasonal scales, while employing temperature and salinity corrections to keep the ocean mean state close to observations (modeling setup as in Hirons et al. (2015)). Therefore, not only are the coupled and atmosphere-only mean states consistent, but, because they are close to observations, there is a limited influence of coupled-model SST errors on our conclusions. A variety of extreme diagnostics have been applied to analyze the impact on the frequency, intensity, and persistence of tropical precipitation extremes during extended summer (MJJAS) and winter (NDJFM) seasons.

We have shown that MetUM-GA3 forced by 31 day smoothed MetUM-GOML1 SSTs overestimates the frequency, intensity, and persistence of tropical precipitation extremes relative to the MetUM-GOML1 simulations that generated the SST forcing. Coupled air-sea interactions damp rainfall variability, leading to less frequent, and intense tropical precipitation extremes (Figures 2e, 2f, 3e, and 3f) that are also shorter-lived (Figures 4e–4h and 5). These changes are seen in both seasons and are not directly linked to a change in the mean rainfall (Figures 1e and 1f). The damping of rainfall variability and extremes with air-sea interactions is likely due to negative local thermodynamic feedbacks in the coupled system through convection, surface fluxes, and SST.

Most of the overestimation of extremes in GA3–31d relative to GOML1 occurs over the tropical oceans, suggesting that the interannual SST variability increases rainfall variability locally, resulting in more intense, longer-lived extremes (Figures 4 and 5). During MJJAS some of this overestimation can be linked to the change to the mean tropical precipitation (Figure 1c), however, during NDJFM this is not the case (Figure 1d). Comparing GA3–31d with GA3-clim demonstrates that SST variability drives the increase in extremes in GA3–31d relative to GOML1. GA3-clim provides an estimate of the non-SST-forced characteristics of

extremes in GA3. Differences between GOML1 and GA3–31d suggest that attribution studies or time-slice experiments employing atmosphere-only models (e.g., Coppola & Giorgi, 2005; Kopparla et al., 2013) may overestimate the intensity and persistence of tropical precipitation extremes because they lack coupled feedbacks. Prescribing SSTs in an atmosphere-only model increases tropical precipitation extremes relative to the coupled model that generated those SSTs in the first place.

Changes in the characteristics of tropical precipitation extremes are not confined to oceanic regions; there are also land regions such as southern India (Figures 2a, 2c, and 3e), northern Africa (Figures 2b, 2d, 3f, 4f, and 4j) and central Australia (Figures 3c, 4e, and 4i) that are sensitive to the inclusion of air-sea interactions. While some studies suggest that air-sea interactions only affect internal variability and would not change the outcome of future projections (e.g., He & Soden, 2016), others have shown that decadal changes in extreme precipitation, especially during the summer monsoons in East Asia and Australia, exhibited considerable sensitivity to air-sea interactions (e.g., Dong et al., 2017). These sensitivities highlight that any conclusions drawn from future modeling studies about the impacts of precipitation extremes, whether of the current or future climate, should be interpreted in the context of the modeling framework used.

MetUM has substantial biases in climatological precipitation over tropical land masses; for example, it does not adequately capture Indian summer monsoon rainfall (Johnson et al., 2015). It also has a weak representation of tropical subseasonal variability; for example, the eastward propagation of the Madden-Julian oscillation is poorly simulated (Klingaman, 2014). It is therefore important to improve understanding of these model deficiencies, as they are likely to affect the representation of tropical precipitation extremes.

It would also be interesting to extend this analysis to other GCMs to investigate the consistency of the impact of air-sea interactions on tropical precipitation extremes. Another potentially illuminating extension of this work would be to investigate the role that air-sea interactions play on the frequency, intensity, and persistence of dry extremes in the tropics.

In the results shown here the oceanic temperature and salinity corrections—required to account for biases in atmospheric surface fluxes and represent mean oceanic advection—have been calculated to produce a near-observed mean state. Similar MetUM-GOML experiments could be conducted for attribution or climate-change studies by recalculating the corrections to reproduce the ocean mean state of any particular year/period (for attribution studies) or future scenario (for climate-change studies).

References

Allan, R. P., & Soden, B. J. (2008). Atmospheric warming and the amplification of precipitation extremes. *Science*, *321*(5895), 1481–1484.

Arribas, A., Glover, M., Maidens, A., Peterson, K., Gordon, M., MacLachlan, C., et al. (2011). The GloSea4 ensemble prediction system for seasonal forecasting. *Monthly Weather Review*, *139*, 1891–1910.

Asadieh, B., & Krakauer, N. Y. (2015). Global trends in extreme precipitation: Climate models versus observations. *Hydrology and Earth System Sciences*, *19*, 877–891.

Bernie, D. J., Woolnough, S. J., & Slingo, J. M. (2005). Modeling dirunal and intraseasonal variability of the ocean mixed layer. *Journal of Climate*, *18*, 1190–1202.

Coppola, E., & Giorgi, F. (2005). Climate change in tropical regions from high-resolution time-slice AGCM experiments. *Quarterly Journal of the Royal Meteorological Society*, *131*, 3123–3145.

DeMott, C. A., Klingaman, N. P., & Woolnough, S. J. (2015). Atmosphere-ocean coupled processes in the Madden-Julian oscillation. *Reviews of Geophysics*, *53*, 1099–1154. https://doi.org/10.1002/2014RG000478

Deser, C., & Phillips, A. S. (2009). Atmospheric circulation trends, 1950–2000: The relative roles of sea surface temperature forcing and direct atmospheric radiative forcing. *Journal of Climate*, *22*, 396–413.

Dong, B., Sutton, R. T., Shaffrey, L., & Klingaman, N. P. (2017). Attribution of forced decadal climate change in coupled and uncoupled ocean-atmosphere model experiments. *Journal of Climate*, *30*(16), 6203–6223.

He, J., & Soden, B. J. (2016). Does the lack of coupling in SST-forced atmosphere-only models limit their usefulness for climate change studies? *Journal of Climate*, *29*(12), 4317–4325. https://doi.org/10.1175/JCLI-D-14-00597.1

Hirons, L. C., Klingaman, N. P., & Woolnough, S. J. (2015). MetUM-GOML1: A near-globally coupled atmosphere-ocean-mixed-layer model. *Geoscientific Model Development*, *8*, 363–379.

Johnson, S. J., Turner, A. G., Woolnough, S. J., Martin, G. M., & Klingaman, N. P. (2015). The effect of increased convective entrainment on Asian monsoon biases in the MetUM General Circulation Model. *Quarterly Journal of the Royal Meteorological Society*, *141*(686), 311–326.

Kharin, V. V., Zwiers, F. W., Zhang, X., & Hegerl, G. C. (2007). Changes in temperature and precipitation extremes in the IPCC ensemble of global coupled model simulations. *Journal of Climate*, *20*, 1419–1444.

Kharin, V. V., Zwiers, F. W., Zhang, X., & Wehner, M. (2013). Changes in temperature and precipitation extremes in the CMIP5 ensemble. *Climatic Change*, *119*, 345–357.

Klingaman, N. (2014). Using a case-study approach to improve the MJO in the Hadley Centre Climate Model (HadGEM). *Quarterly Journal of the Royal Meteorological Society*, *140*(685), 2491–2505.

Klingaman, N. P., Woolnough, S. J., Weller, H., & Slingo, J. M. (2011). The impact of finer-resolution air-sea coupling on the intraseasonal oscillation of the Indian Monsoon. *Journal of Climate*, *24*, 2451–2468.

Kopparla, P., Fischer, M. E., Hannay, C., & Knutti, R. (2013). Improved simulation of extreme precipitation in a high-resolution atmosphere model. *Geophysical Research Letters*, *40*, 5803–5808. https://doi.org/10.1002/2013GL057866

O'Gorman, P. A. (2015). Precipitation extremes under climate change. *Current Climate Change Reports*, *1*(2), 49–59.

O'Gorman, P. A., & Schneider, T. (2009). The physical basis for increases in precipitation extremes in simulations of 21st-century climate change. *Proceedings of the National Academy of Sciences of the United States of America*, *106*(35), 14,773–14,777.

Pegion, K., & Kirtman, B. P. (2008). The impact of air-sea interactions on the simulation of tropical intraseasonal variability. *Journal of Climate*, *24*, 6616–6635.

Rajendran, K., & Kitoh, A. (2006). Modulation of tropical intraseasonal oscillations by ocean-atmosphere coupling. *Journal of Climate*, *19*, 366–391.

Ratnam, J. V., Morioka, Y., Behera, S. K., & Yamagata, T. (2015). A model study of regional air-sea interaction in the austral summer precipitation over southern Africa. *Journal of Geophysical Research: Atmosphere*, *120*, 2342–2357. https://doi.org/10.1002/2014JD022154

Ringer, M. A., Martin, G. M., Greeves, C. Z., Hinton, T. J., James, P. M., Pope, V. D., et al. (2006). The physical properties of the atmosphere in the New Hadley Centre Global Environmental Model (HadGEM1). Part II: Aspects of variability and regional climate. *Journal of Climate*, *19*, 1302–1326.

Rossow, W. B., Mekonnen, A., Pearl, C., & Goncalves, W. (2013). Tropical precipitation extremes. *Journal of Climate*, *26*, 1457–1466.

Schar, C., Ban, N., Fischer, E. M., Rajczaj, J., Schmidli, J., Frei, C., et al. (2016). Percentile indices for assessing changes in heavy precipitation events. *Climatic Change*, *137*, 201–216.

Senevirante, S. I., Nicholls, N., Easterling, D., Goodess, C. M., Kanae, S., Kossin, J., et al. (2012). Changes in climate extremes and their impacts on the natural physical environment. In *Managing the risks of extreme events and disasters to advance climate change adaptation. A special report of working groups I and II of the Intergovernmental Panel on Climate Change* (pp. 109–230). Cambridge, UK: Cambridge University Press.

Smith, D. M., & Murphy, J. M. (2007). An objective ocean temperature and salinity analysis using covariances from global climate models. *Journal of Geophysical Research*, *112*, C02022. https://doi.org/10.1029/2005JC003172

Spencer, H., & Slingo, J. M. (2003). The simulation of peak and delayed ENSO teleconnections. *Journal of Climate*, *16*, 1757–1774.

Tseng, W.-L., Tsuang, B.-J., Keenlyside, N. S., Hsu, H.-H., & Tu, C.-Y. (2015). Resolving the upper-ocean warm layer improves the simulation of the Madden-Julian oscillation. *Climate Dynamics*, *44*(5–6) 1487–1503. https://doi.org/10.1007/s00382-014-2315-1

Walters, D. N., Best, M. J., Bushell, A. C., Copsey, D., Edwards, J. M., Falloon, P. D., et al. (2011). The Met Office Unified Model Global Atmosphere 3.0/3.1 and JULES Global Land 3.0/3.1 configurations. *Geoscientific Model Development*, *4*, 919–941.

Wilcox, E. M., & Donner, L. J. (2006). The frequency of extreme rain events in satellite rain-rate estimated and an atmospheric general circulation model. *Journal of Climate*, *20*, 53–69.